BNL-90931-2010-TECH
EIC/23;BNL-90931-2010-IR

R&D ERL: HTS Solenoid

R. Gupta,

January 2010

Collider Accelerator Department
Brookhaven National Laboratory

U.S. Department of Energy
USDOE Office of Science (SC)

DISCLAIMER

BNL-90931-2010-IR

C-A/AP/#377
January 2010

R&D ERL: HTS Solenoid

R. Gupta, J. Muratore, S. Plate

Collider-Accelerator Department
Brookhaven National Laboratory
Upton, NY 11973

HTS Solenoid for Electron Recovery Linac

Ramesh Gupta, Joseph Muratore and Stephen Plate

Overview

An innovative feature of the ERL project is the use of a solenoid made with High Temperature Superconductor (HTS) with the Superconducting RF cavity. The HTS solenoid design offers many advantages because of several unique design features. Typically the solenoid is placed outside the cryostat which means that the beam gets significantly defused before a focusing element starts. In the current design, the solenoid is placed inside the cryostat which provides an early focusing structure and thus a significant reduction in the emittance of the electron beam. In addition, taking full advantage of the high critical temperature of HTS, the solenoid has been designed to reach the required field at ~77 K, which can be obtained with liquid nitrogen. This significantly reduces the cost of testing and allows a variety of critical pre-tests which would have been prohibitively expensive at 4 K in liquid helium because of the additional requirements of cryostat and associated facilities.

1. Overall and Magnetic Design

The solenoid is placed between the superconducting gun cavity and the gate valve (Fig. 1.1). Compared to a room temperature magnet, the HTS solenoid makes overall design much simpler and technically superior. With the smaller beam pipe size possible, HTS significantly reduces the amount of material needed to make the coil and greatly reduces the power needed to drive the magnet and subsequently the heat generated during its operation. The solenoid is situated in the transition region (4 K to room temperature) where the temperature is expected to be too high for a conventional low temperature superconductor.

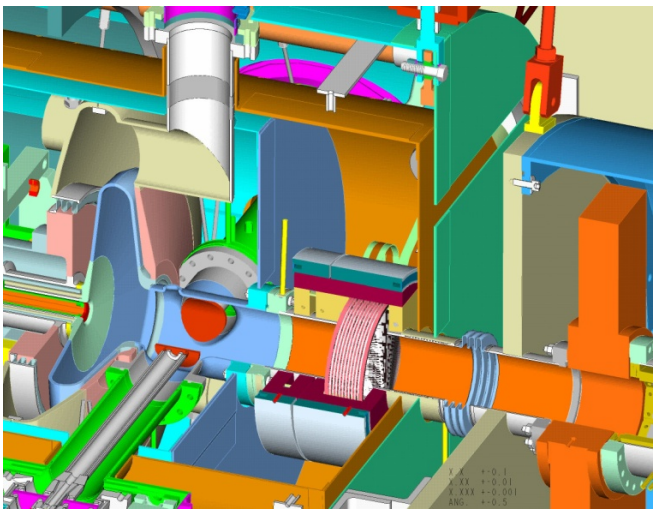

Fig. 1.1 Main coil (layer-wound, in front) and bucking coil (double pancake, in back) of the HTS solenoid for the ERL project.

In addition to the main coil, the solenoid includes a bucking coil to minimize the field on the superconducting RF cavity. Additional shielding between the solenoid and cavity ensure very low field. In fact, assuring that the trapped field is below the milli-Gauss level on the superconducting cavity has been a major design consideration.

The main coils are placed over the bellows, so little additional space is consumed. The majority of the field is generated by the iron which has a much smaller inner radius than the coils (see Table I). The main coil is a layer-wound coil with 180 turns in 15 layers and the bucking coil is a double pancake coil with a total of 30 turns. All coils are made with helically wrapped-Kapton, insulated BSCCO-2223 tape supplied by American Superconductor Corporation [1]. Major parameters of the solenoid are given in Table I. The nominal integrated axial focusing strength is ~1 T^2. mm.

TABLE I MAJOR PARAMETERS OF HTS SOLENOID FOR ERL

Parameters	**Value**
Coil Inner Diameter	175 mm
Coil Outer Diameter	187 mm
No. of Turns in Main Coil	180
No. of Turns in Bucking Coil	30 (2X15)
Coil Length (Main Coil)	~56 mm
Coil Length (Bucking Coil)	~9 mm
Conductor (First Generation HTS)	BSCCO2223 Tape
Insulation	Kapton
Total Conductor Used	118 meter
Nominal Integral Focusing	1 T^2. mm (axial)
Nominal Current in Main Coil	54.2 A
Nominal Current in Bucking Coil	-17 A
Max. Field on Conductor, Parallel/Perpendicular	0.25 T/0.065 T
Stored Energy	~25 Joules
Inductance (main coil)	0.13 Henry
Yoke Inner Radius	55 mm
Yoke Outer radius	114 mm
Yoke Length (Main + Bucking)	147 mm

Magnetic Design

Overall magnetic design of the solenoid and superconducting cavity is shown in Fig 1.2. Magnetic field calculations include the influence of the shielding provided by the superconducting cavity.

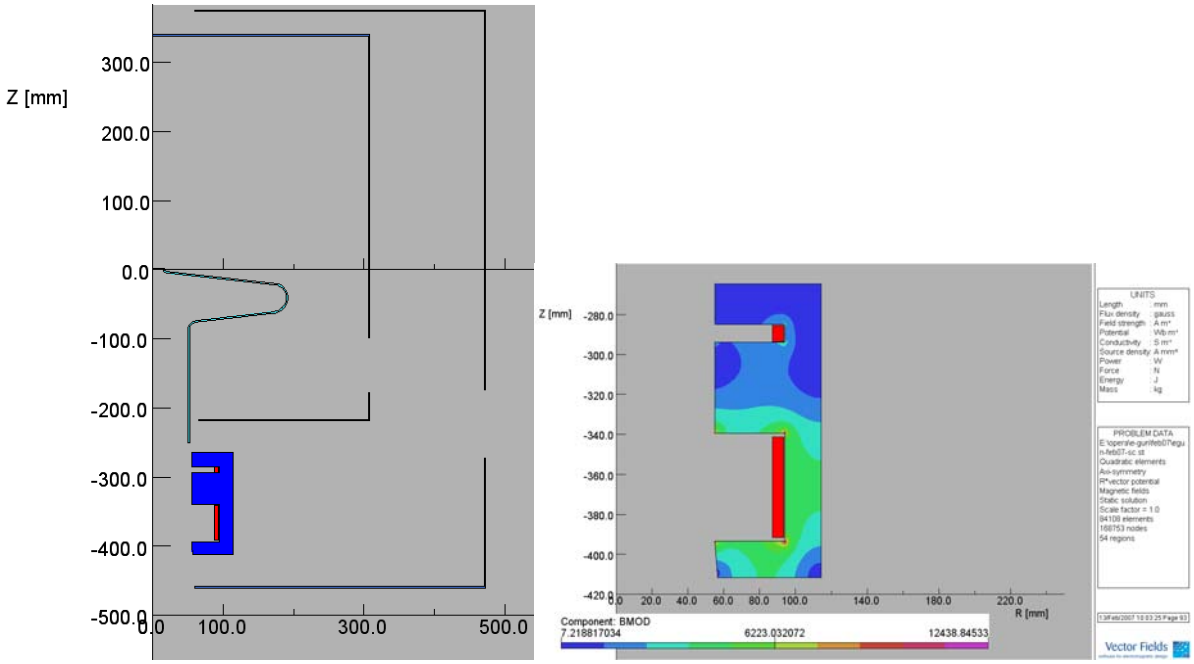

Fig. 1.2. Overall magnetic design of the solenoid with inner magnetic shield and superconducting cavity (left) and the magnitude of the field in the iron yoke (right).

The solenoid is placed as close to the superconducting cavity as possible. Moreover, to reduce the length of the cryostat, the superconducting coil has been placed over the bellows (see Fig 1.3). The design shown here is the iterated version of several concepts which included solenoid coils with different inner radii and designs with and without iron enclosure (yoke). Apart from minimizing the axial size, convenience of the overall assembly also played a significant role in optimizing various concepts and parameters of the design.

The strength of the field and variation along the axis is primarily determined by the iron (particularly at the inner radius near the coil). There is a slide angular wedge on the side away from the cavity for the edge of installation. Magnetic analysis shows that this can be tolerated.

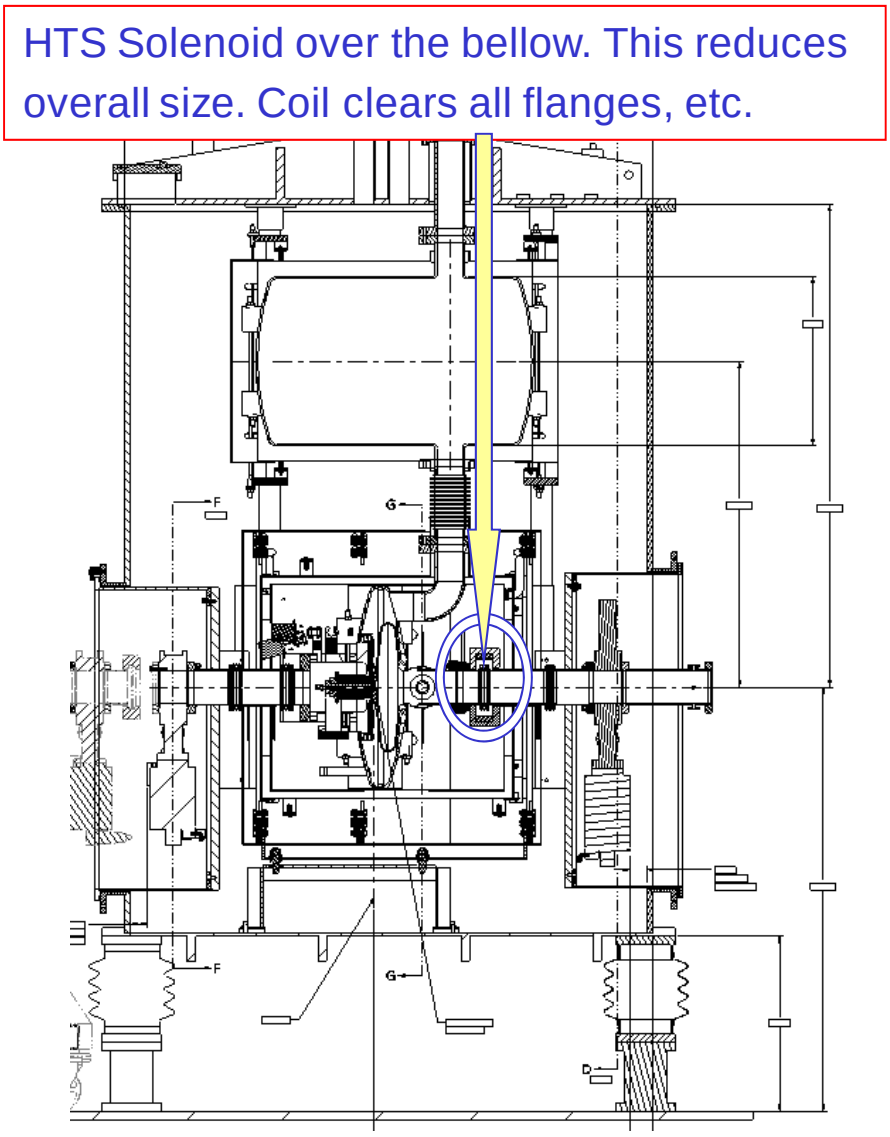

Fig. 1.3. The solenoid is placed over the bellows to reduce the length of the cryostat.

The basic design requirement of the solenoid is that it provides the following overall integral focusing with the axial component of the field:

$$\int B_z^2 dz \approx 1\ T^2\ .\ mm$$

The computed map and the axial profile of the focusing by the solenoid coil are shown in Fig. 1.4. These calculations include the shielding provided by the superconducting region of the cavity.

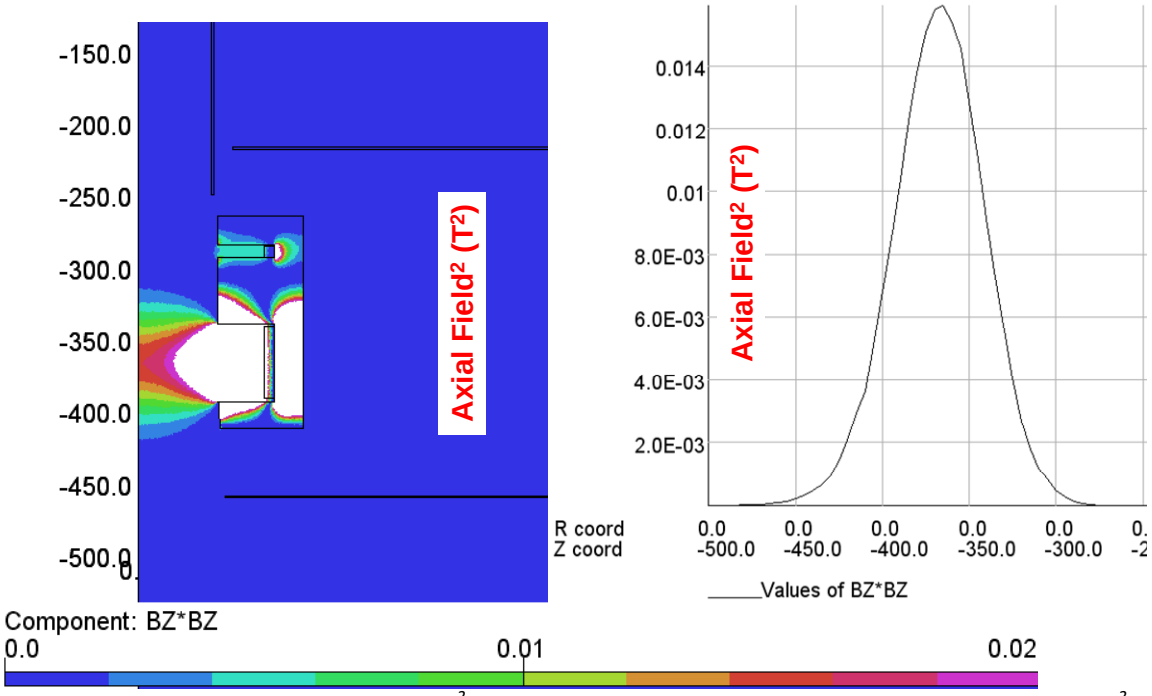

Fig. 1.4. Computed map of the focusing (B_z^2) is shown on the left and the axial profile of the focusing (B_z^2) along the beam axis is shown on the right.

Even though the shielding provided by the superconducting structure reduces the field at the entrance of cavity was still higher than acceptable, and therefore the bucking coil (as shown in the model) was introduced in the design. Whereas the larger main coil has 180 turns, the bucking coil has only 30. Moreover, the bucking coil runs at a significantly lower current in the nominal design (for 54.2 A in the main coil, the bucking coil will have -17 A). Fig. 1.5 shows the magnitude of the field inside the axis of cavity with and without bucking coil. Beam is injected in the cavity at z=0 and travels downward in the negative z-direction.

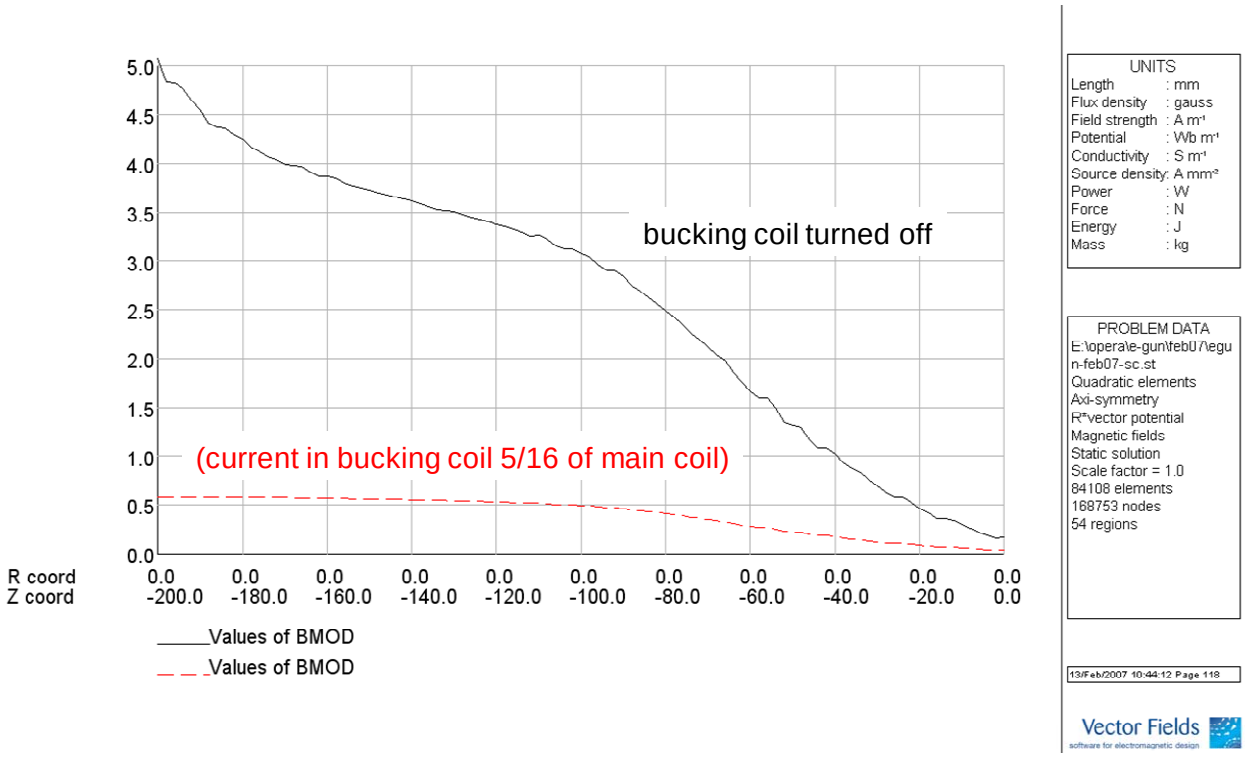

Fig.1.5. Magnitude of the field inside the axis of cavity with and without bucking coil. Current in the bucking coil can be adjusted to further minimize the field at the center or at the surface of the cavity.

The main and bucking coils are connected with independent power supplies so as to change the ratio from the nominal value of 5/16 in order to experimentally optimize the performance during the operation.

An important consideration in the design is to make sure that the field on the cavity remains below 10 mG during the operation. This is to minimize the trap field on the superconducting cavity which could limit its operation. An inner magnetic shield (as shown in Fig. 1.6 and also in Fig. 1.1) is placed between the solenoid and the cavity to reduce the leakage field on the cavity from the solenoid.

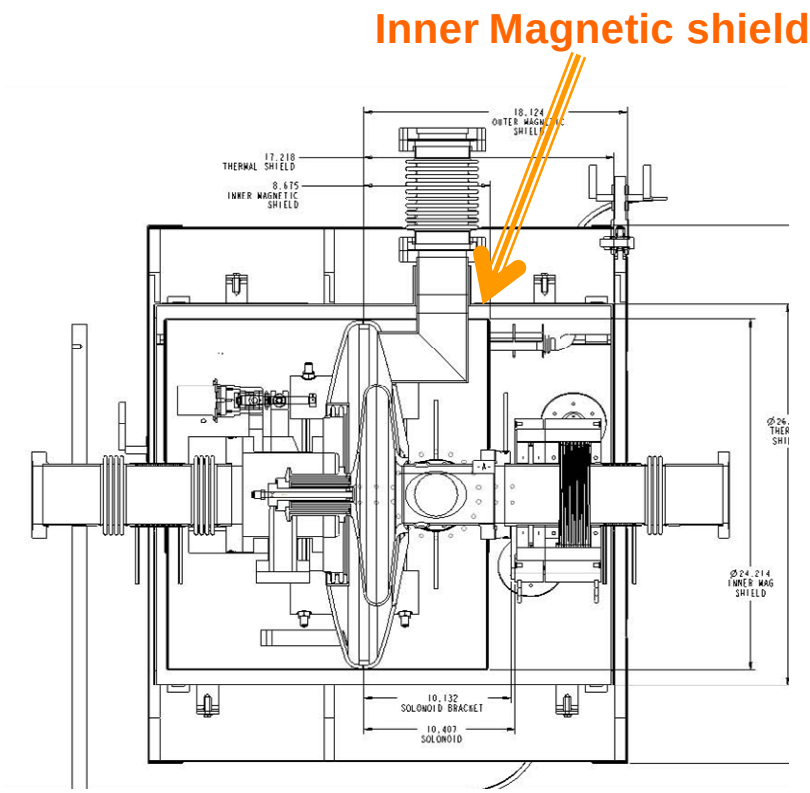

Fig. 1.6. An inner magnetic shield to minimize the leakage field on the superconducting cavity from the solenoid.

The bucking coil in the solenoid plays an important role in reducing the leakage field on the cavity as well. Fig. 1.7 shows the field map with the bucking solenoid turned on at the nominal current (left) and turned off (right). One can clearly see the reduction in field inside the cavity. One can also see the reduction in leakage field on the cavity and inside the inner magnetic shield.

Fig. 1.8 shows the field on the surface of superconducting cavity based on a model superconducting shield. The reliability of these models is unknown at the level of 10 mG (1 micro Tesla). An experimental program has been initiated to measure the leakage field given the critical nature of this issue. These measurements are being performed at ~77 K in liquid nitrogen. The superconducting cavity will not be in place during these measurements. Fig. 1.9 shows the expected fringe field in the absence of the superconducting shield from the cavity (for reference purpose, an outline shows the location of the cavity). This simulates the present test setup only. In the actual operating case the superconducting cavity will be present and the superconducting surface will prohibit field penetration and hence provide shielding, Flux will, still leak through the inner bore tube as the entire volume is not fully enclosed by the superconducting shield. The case shown in Fig. 1.9 does not represent the exact optimized ratio of the current between the bucking and main coil. The exact ratio will be determined experimentally. Because of the

superconducting shielding, it is not necessary that the same ratio will minimize the field on the surface of cavity and at the entrance region of the beam.

The testing at ~77K with liquid nitrogen makes these measurements affordable and practical. As mentioned earlier, the HTS solenoid has been designed to reach the critical performance in liquid nitrogen itself even though the temperature would be well below 20 K in actual operating condition.

Field inside cavity with bucking coil excited
(current in bucking coil 5/16 of main coil)

Field inside cavity with bucking coil turned off

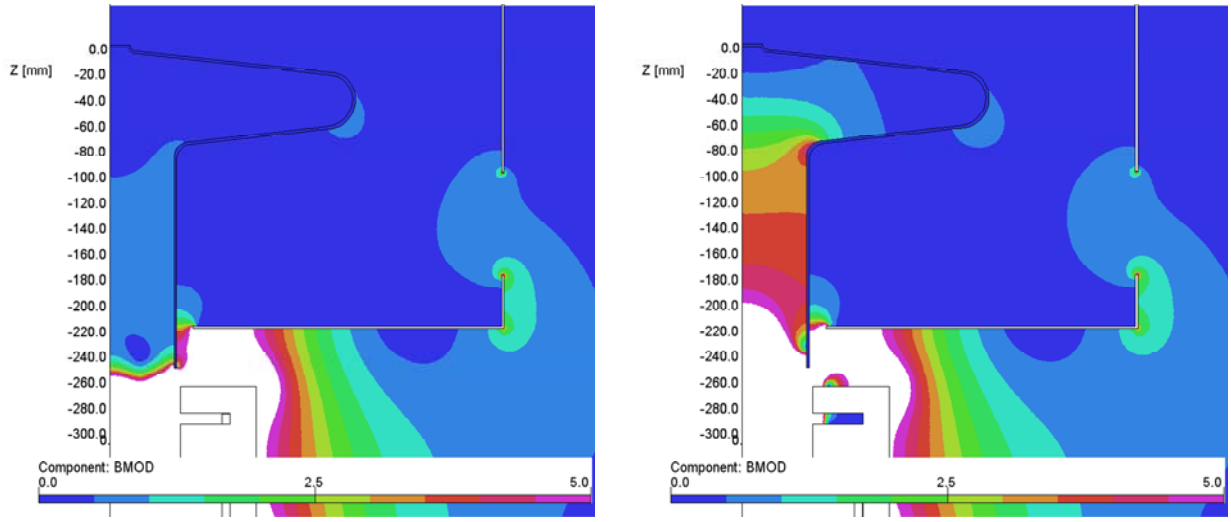

Fig. 1.7. Field map (in Gauss) with the bucking solenoid turned on at the nominal current (left) and turned off (right). One can clearly see the reduction in field inside the cavity. One can also see the reduction in leakage field on the cavity and inside the inner magnetic shield.

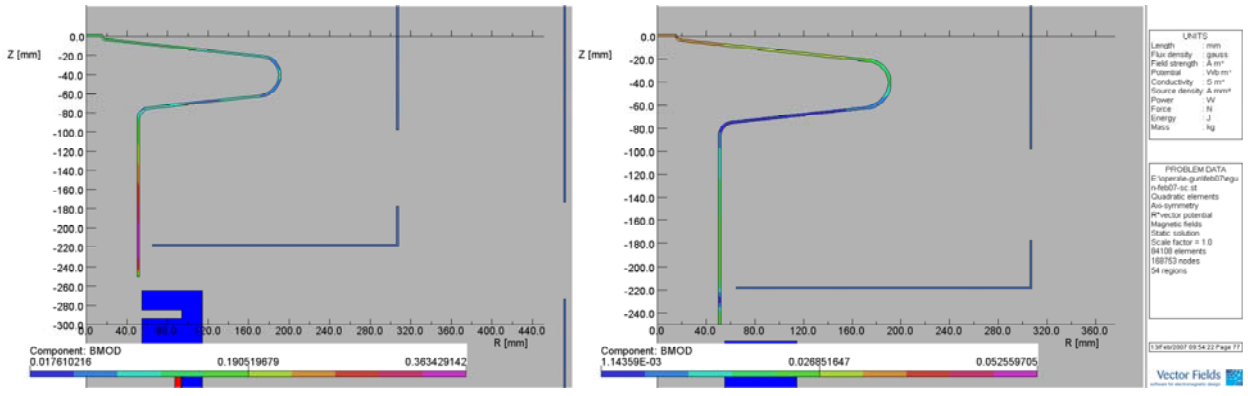

Fig. 1.8. Field (in Gauss) on the surface of superconducting cavity based on a model superconducting shield with the bucking solenoid turned on at the nominal current (left) and turned off (right). One can clearly see a reduction. However, given the sensitive nature of these calculations, magnetic measurements are planned at ~77 K.

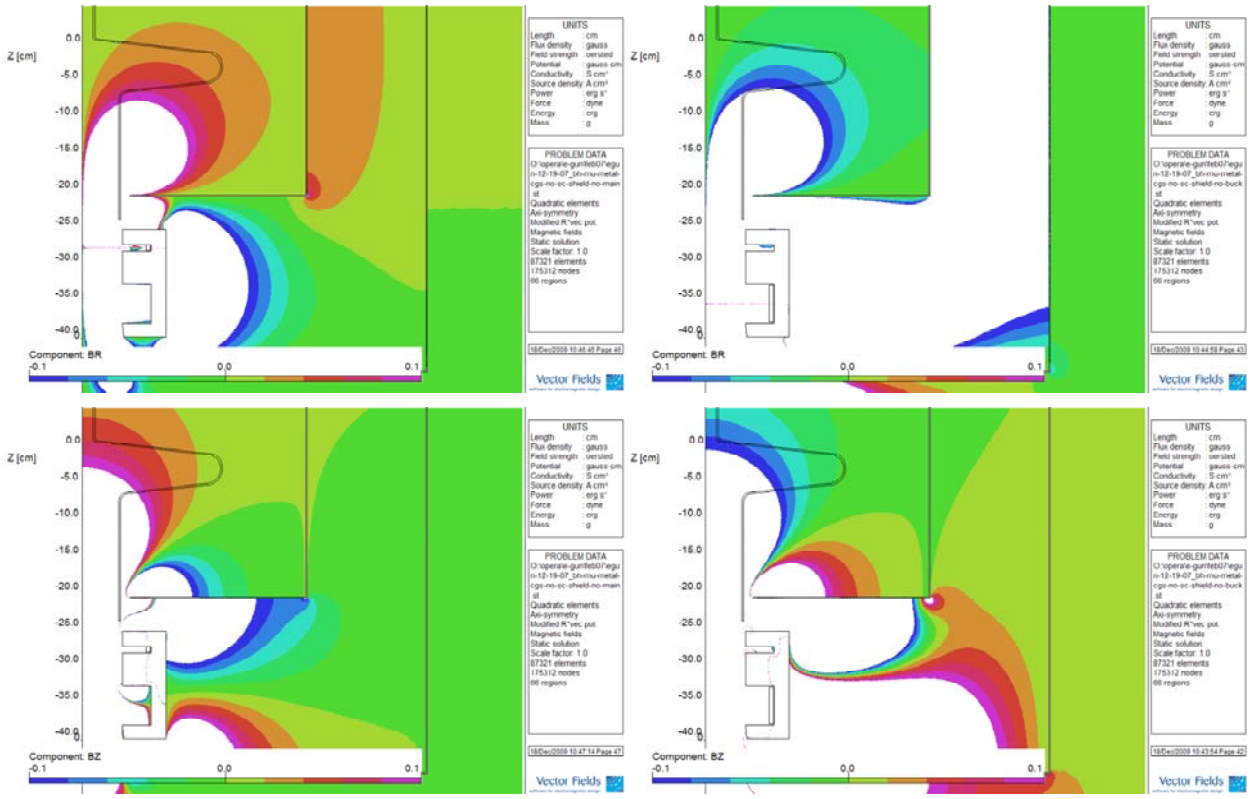

Fig. 1.9. Field map (in Gauss) of radial (upper two) and axial components (lower two) of the solenoid when either main coil is energized (right two) or bucking coil is energized (left two) at the nominal current. Please note the sign and magnitude of the field components near the cavity region. Please also note that there is no shielding from the superconducting cavity. Outline of the superconducting cavity is for reference only. This simulates the present test setup without the superconducting cavity. Superconducting surface prohibits the field penetration and hence provide modifies the field map, particularly inside the cavity region. These measurements are crucial in assuring that the field on the surface of superconducting cavity remains below ~10 mG during the operation. The above case does not represent the exact optimized ratio of the current between the bucking and main coil. The exact ratio will be determined experimentally.

Performance and Test of HTS Coils

Fig. 1.10 shows the HTS coils for the solenoid. The main coil (the larger coil) was layer wound with 180 turns. The bucking coil was wound in double layer pancake with 30 turns and a perpendicular splice at the inner radius.

The first important step was to test these coils at liquid nitrogen without the iron yoke. Interestingly the HTS coils are expected to carry less current in the absence of the yoke. This is because of the fact that the current carrying capacity of HTS depends not only on the magnitude of the field but on the direction of the field relative to tape surface as well. In fact, as shown in Fig. 1.11, direction plays a very large role in determining current carrying capacity (or critical current) at a given temperature and field. The current carrying capacity is significantly smaller

when the field is perpendicular to the surface as compared to when it is parallel. The magnetic design of the solenoid yoke has been optimizes such that the field becomes nearly parallel to the surface of the conductor (see Fig. 1.12 and Fig. 11.13). This not only increases the field on the axis of the solenoid at the given current, but also significantly increases the current carrying capacity of the HTS solenoid coils.

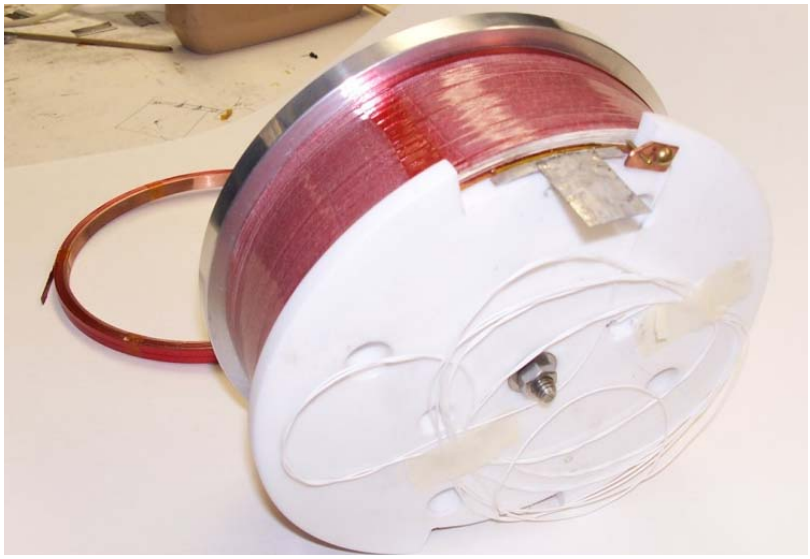

Fig. 1.10. HTS main solenoid coil for the proposed ERL project in a test fixture.

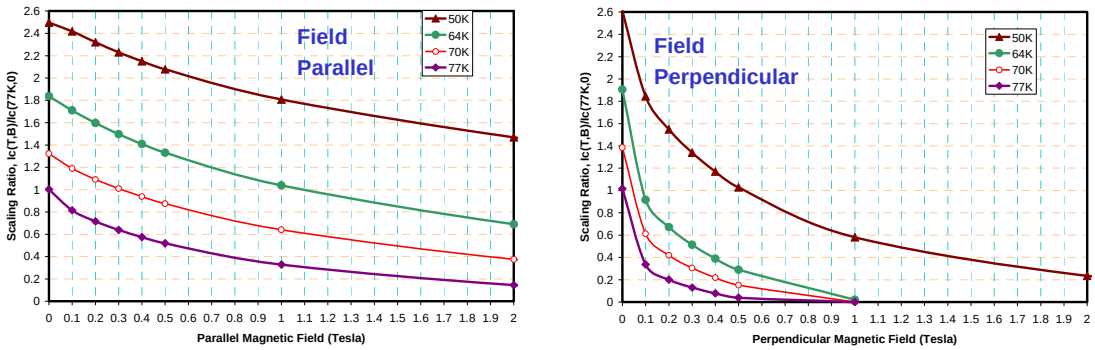

Fig. 1.11. Scaling ratio of critical current at a various temperatures and field with applied field parallel to and perpendicular to tape surface [1]. One can see that HTS is highly anisotropic.

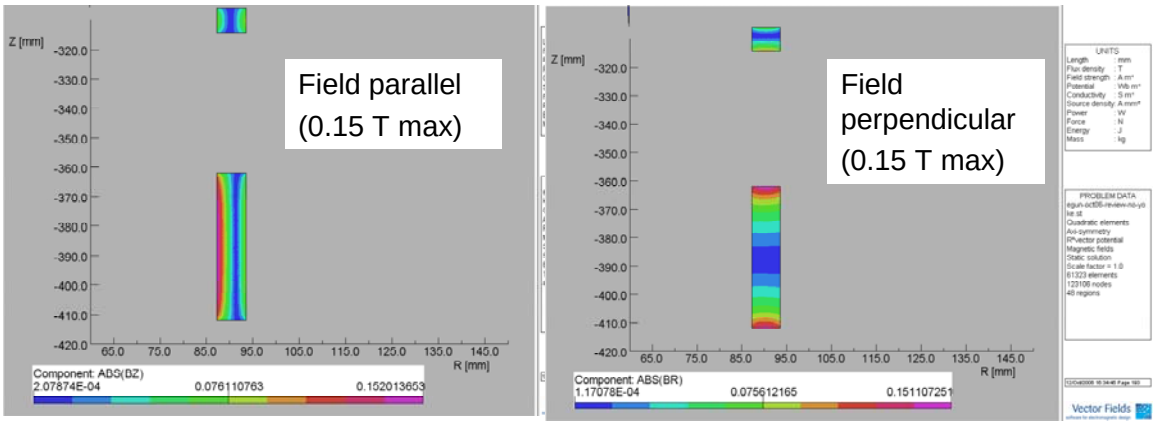

Fig. 1.12. Parallel to and perpendicular components of the fields on surface of HTS tape in the absence of yoke iron.

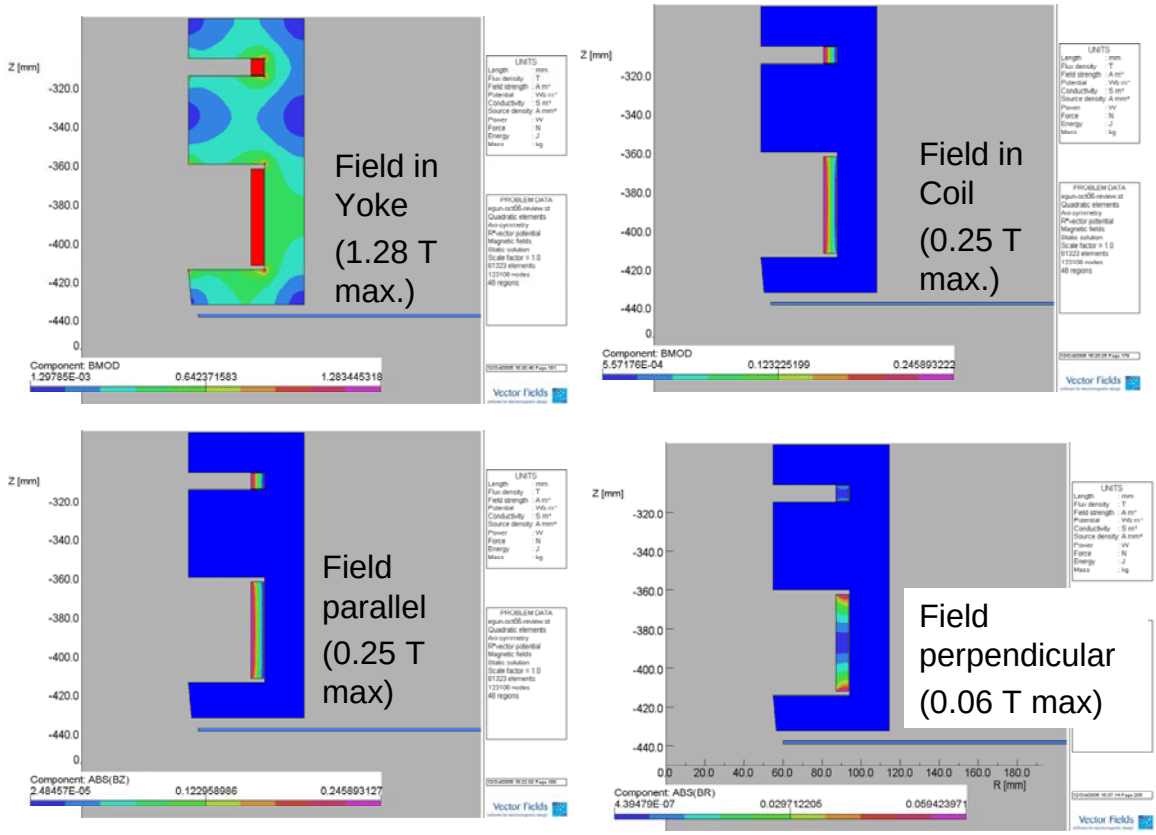

Fig. 1.13. Parallel and perpendicular components of the fields on surface of HTS tape in the presence of yoke iron. One can see that the iron has significantly reduced the perpendicular component of the field (compare to the case of no iron in Fig 1.12), increasing the critical current of the solenoid.

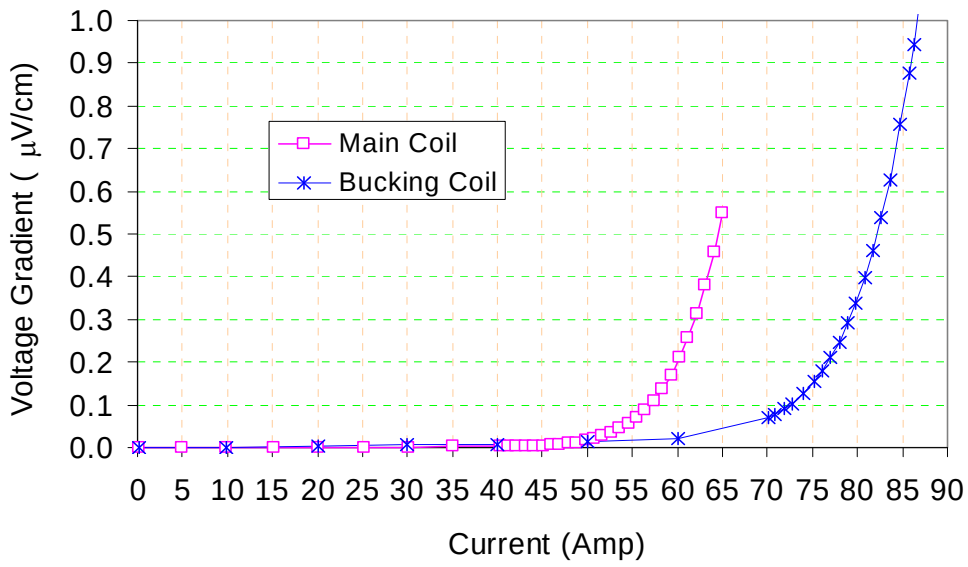

Fig.1.14. Measured voltage gradient at 77 K of the main coil (l80 turns) and the bucking coil (30 turns) HTS solenoid for the proposed ERL project. Both coils were run above the design current at 77K despite the absence of yoke which further increases the critical current .

Fig. 1.14 shows the voltage current characteristics of the main and bucking coils when the measurements are carried out at 77 K (liquid nitrogen). The main coil has an I_c of 54 A and the bucking coil 72 A, respectively, when I_c is specified for a gradient of 0.1 μV/cm (typical definition of I_c is for 1 μV/cm where the current in the main coil will be above 65 A). The lower I_c in the main coil is due to the higher field. In the actual magnet structure, iron would make the field more parallel to the HTS tape which would increase I_c of both coils. Clearly both coils meet the design value of ~54 A even in the absence of yoke. The margin in operating conditions will actually be much greater as the temperature will be well below 77 K. The solenoid could, in principle, have been designed with fewer turns but the desire to use lower current HTS leads motivated a low operating current and a larger number of turns to reach the required Amp-turns. In this case the strength of the solenoid is determined by the iron that has a smaller inner radius than the coil.

2. Engineering Design and Construction

Mechanical

The ERL Superconducting RF Solenoid is comprised of two solenoid coils joined into one assembly: a main coil and an auxiliary or bucking coil. Both coils have the same nominal outer and inner diameters (7.40 and 6.87 inches, respectively), but the main coil is substantially wider (2.20 inches) than the auxiliary coil (0.34 inches). Each coil assembly has an individual low-carbon steel yoke. The complete assembly with its external power leads is shown in Fig. *2.**1***, which also shows a slice of the heat shield (cyan) for understanding, although the shield is not part of the BNL design scope. Both coils use BSSCO alloy "1st generation" HTS superconductor whose cross section is .165 x .015 inches. The nominal operating current for the main coil is 54 Amperes. Both coils and their leads are designed for this current.

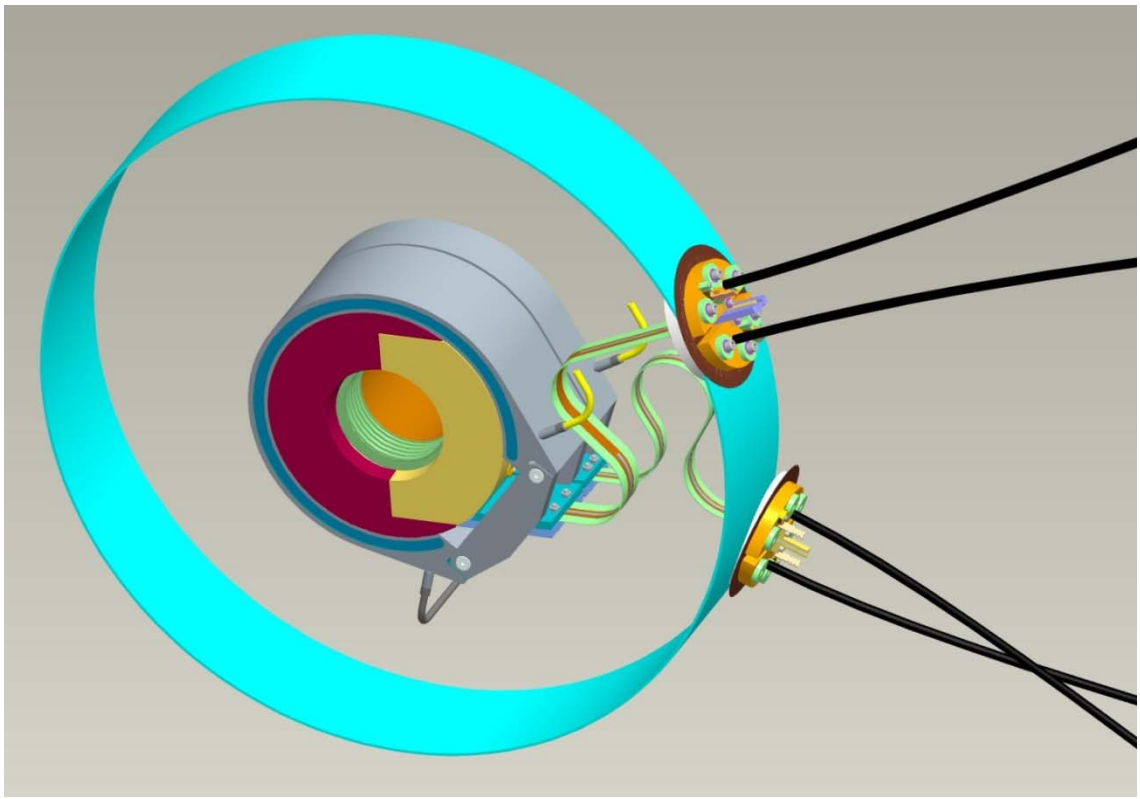

Fig. 2.1 Solenoid Assembly - shown inside a portion of heat shield

The solenoid coils are wound using two different techniques. The main coil is wound in a back and forth level-wind fashion (like line on a fishing reel) so that each layer is laid down as a butt-wrapped helix. Long thin triangular filler pieces, shaped into a three-quarter circle, are placed in the gaps at the end of each layer to maintain a uniform diameter upon which the next layer then rests. There are 12 turns in each layer and 14 layers that make up the main coil. The auxiliary coil is pinwheel wound as two separate pancakes placed face-to-face that are spliced at the inside diameter. To create the correct field orientation, one pancake is wound clockwise and the other counter-clockwise. Each pancake has 14 turns (layers). The leads exiting both the main and auxiliary coils have a tangential orientation, exit in the same direction, and all four leads are essentially co-planar.

The yokes capture their respective coils on the outside diameter and the two sides of each coil. The close fit on the sides locates the coils axially. The fit of each yoke ID to its coil OD is designed to provide moderate pressure to the coil OD both at room temperature and at operating temperature (anywhere between 4K and 50K). To this end the OD of each coil was sized to its yoke using a special thermally conductive epoxy[i] that retains some flexibility at cryogenic temperatures. This mating fit at the diameter interface provides good thermal transfer from the yoke during cooldown and during operation, and provides mechanical support in addition to the relatively thin coil overwrap, thus preventing conductor motion that could causes quenching. The yokes for each coil are split into two unequal pieces as shown in Fig. *2.**2***.2. This is done to accommodate the tangentially exiting coil leads (not all are shown), to help make assembly possible, and to accommodate the differential thermal contraction between the coils and the yokes so that they remain in contact during cooldown. The yokes are assembled with a room temperature gap of .020 inches along the vertical midplane.

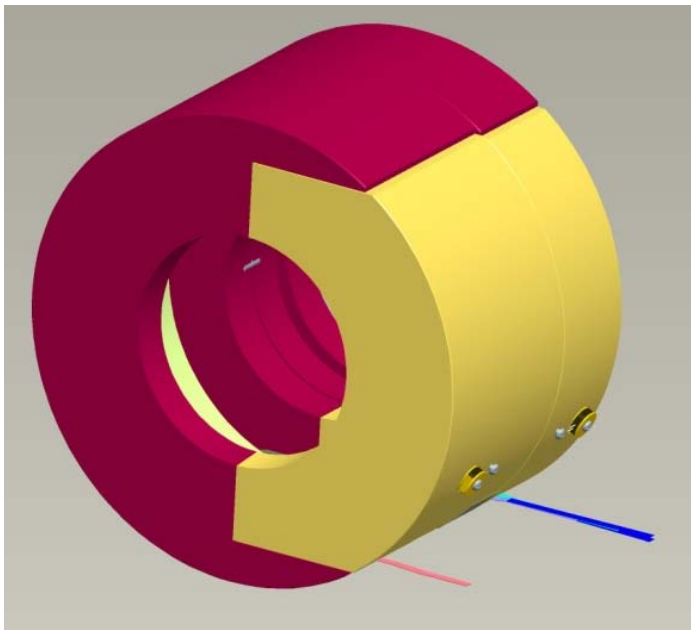

Fig. 2.2 Split Yokes

Surrounding the steel yokes are nearly full-circle aluminum yoke collars. The collars press the two halves of each yoke together during cooldown and are the primary means of directly cooling the yokes, and indirectly the coils. The nominal .020 inch gap that exists between the yoke halves at room temperature is nearly closed at operating temperature due to the greater thermal contraction of the aluminum collar on the outside and the coils inside. The aluminum collars are prevented from spreading open by the attachment of keeper bars across the opening.

The collars are cooled by way of single phase Helium at ~4K passing through a series of small circumferential channels cut into the collar faces, shown teal-colored in

Fig. *2.**3***. Aluminum-to-stainless steel transition tube stubs are pre-welded to the aluminum collars (and leak checked) to allow stainless tubing to be connected after the solenoid is incorporated into the RF gun assembly.

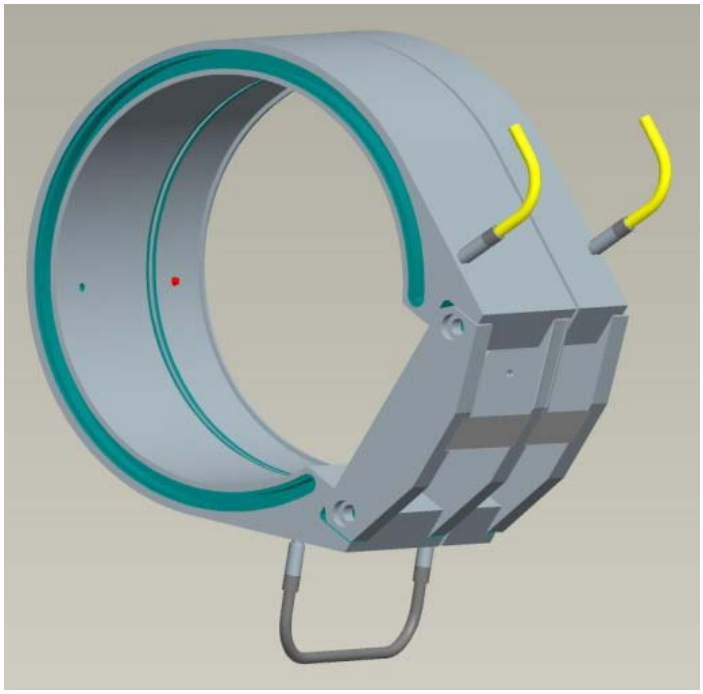

Fig. 2.3 Yoke collars

The coils are aligned and restrained rotationally with respect to the yokes via the exiting leads and by compression at the OD of the coil. The yokes and collars are aligned with respect to each other via set screws through the collars that extend minimally into recesses in the yokes. When incorporated into the entire RF gun assembly, the solenoid assembly is indexed axially and rotationally relative to the RF

cavity by features on the solenoid assembly that mate with complementing features on a protruding flange on the beam tube OD.

Electro-Mechanical

Once the coil leads exit the tangential slot between mating yoke halves, they are protected from damage by entering flat G-10 splice boxes. The boxes are made in two halves. Inside the boxes are shaped pockets that anchor the splices joining the coil leads to pre-fabricated and tested HTS flexible lead assemblies.

Fig. *2.**4*** shows an open box with a 6-strip splice inside. The straight lead (pink) is from the coil; the curved lead (grey) is part of the flex assembly. The rest of the flex lead assembly has been hidden for clarity.

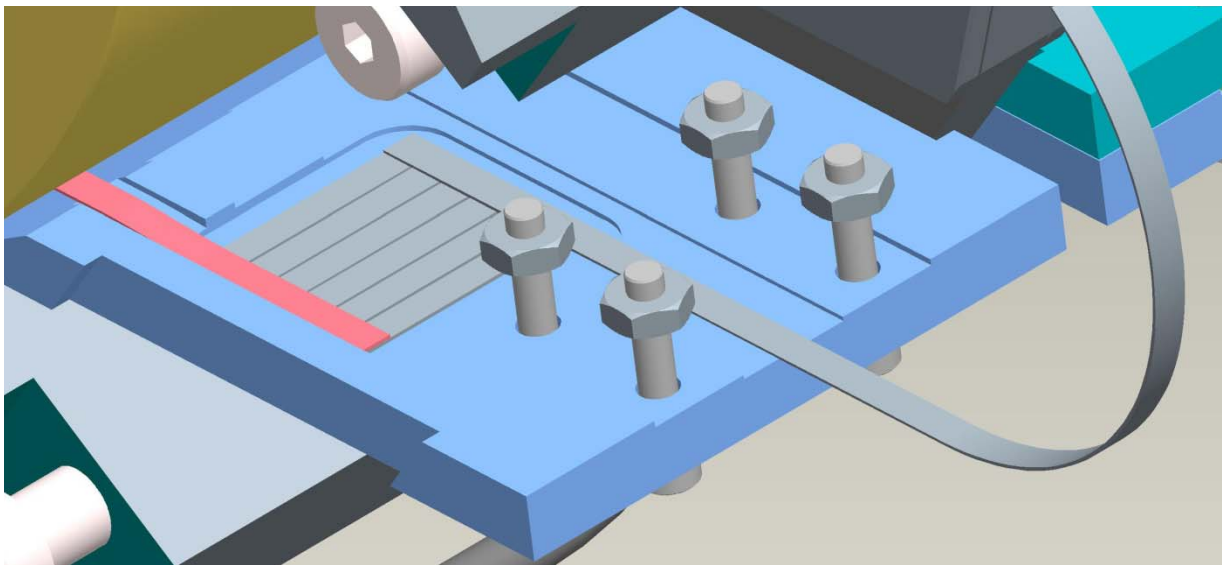

Fig. 2.4 Splice Box (main coil)

The flexible lead assemblies use the same BSSCO alloy as the coils. The lead assemblies are constructed as a sandwich. Two pieces of .015 inch thick G-10 are glued together face-to-face in a laminating jig, creating a shaped spine for the flex leads. When cured and removed from the jig, the spine holds the desired shape for the flex leads. Two layers of .002 inch thick Kapton are applied to opposite faces of the spine. Opposite polarity leads are placed on the outside faces of the Kapton, and another two layers of .002 inch thick Kapton are applied over each lead, thus encapsulating the lead. The main and auxiliary coils each have their own lead set, resulting in four exiting leads that are available for powering either as a series-connected circuit or with separate power supplies. Figure 2.5 shows a lead assembly (outer Kapton over HTS removed for clarity).

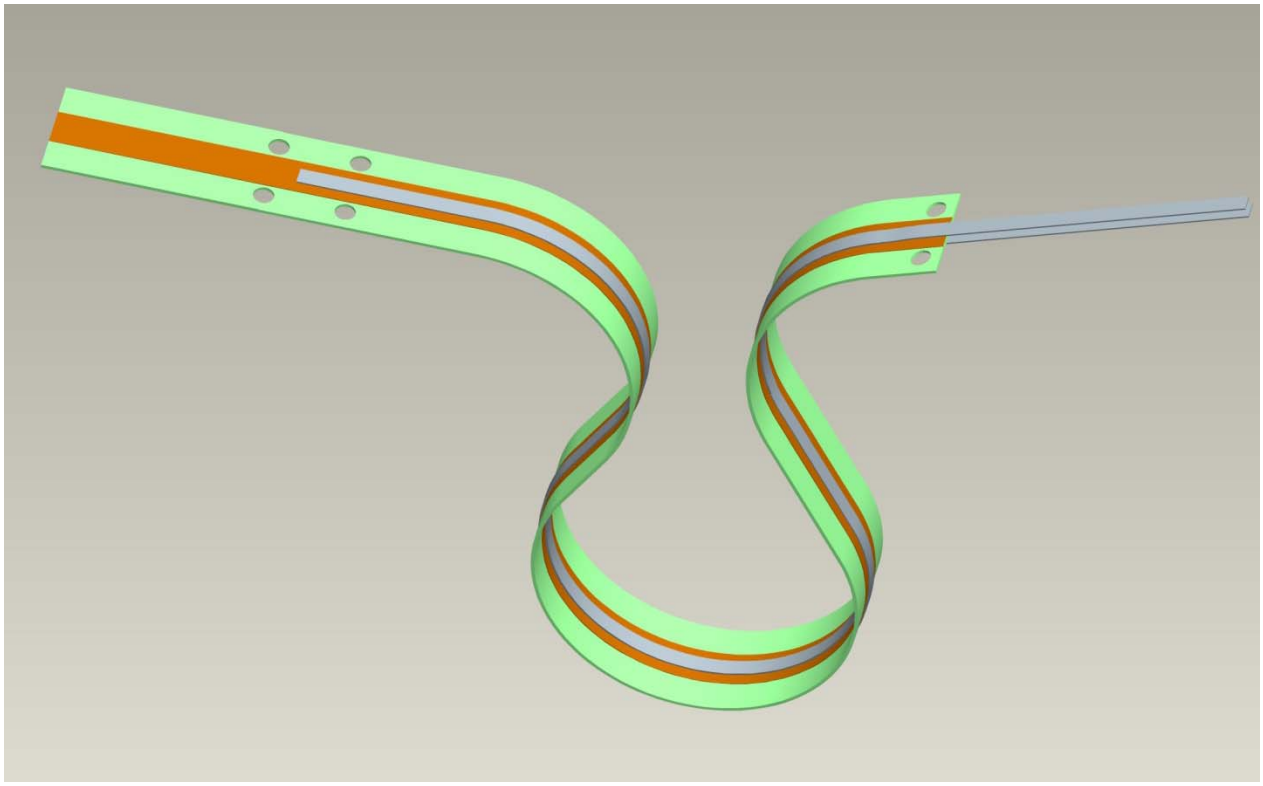

Fig. 2.5 Lead Assembly (auxiliary coil)

The “warm” ends of each HTS flex lead assembly are attached to a copper terminal set. Each terminal set serves as the division point between HTS and the copper wire conductors that eventually extend outside the insulating vacuum space. Beyond each terminal set, 6 AWG wires carry the current. Each terminal set is heat stationed to the heat shield (T=~80K), but electrically isolated from it, by using two sheets of .005 thick Kapton between the terminal and a mating heat shield boss, and by using insulating bushings around the attachment hardware . There are two such heat shield bosses, one for each lead assembly set (main or auxiliary coil set), and they are positioned on the shield in different azimuthal locations to eliminate physical interference between them (refer to Fig. *2.**1***). Each heat shield boss is made as a two-part “clamp” so that the heat shield is sandwiched in this clamp. A side view of the entire heat station, with an axial slice of the shield clamped, is shown in Fig. *2.**6***.

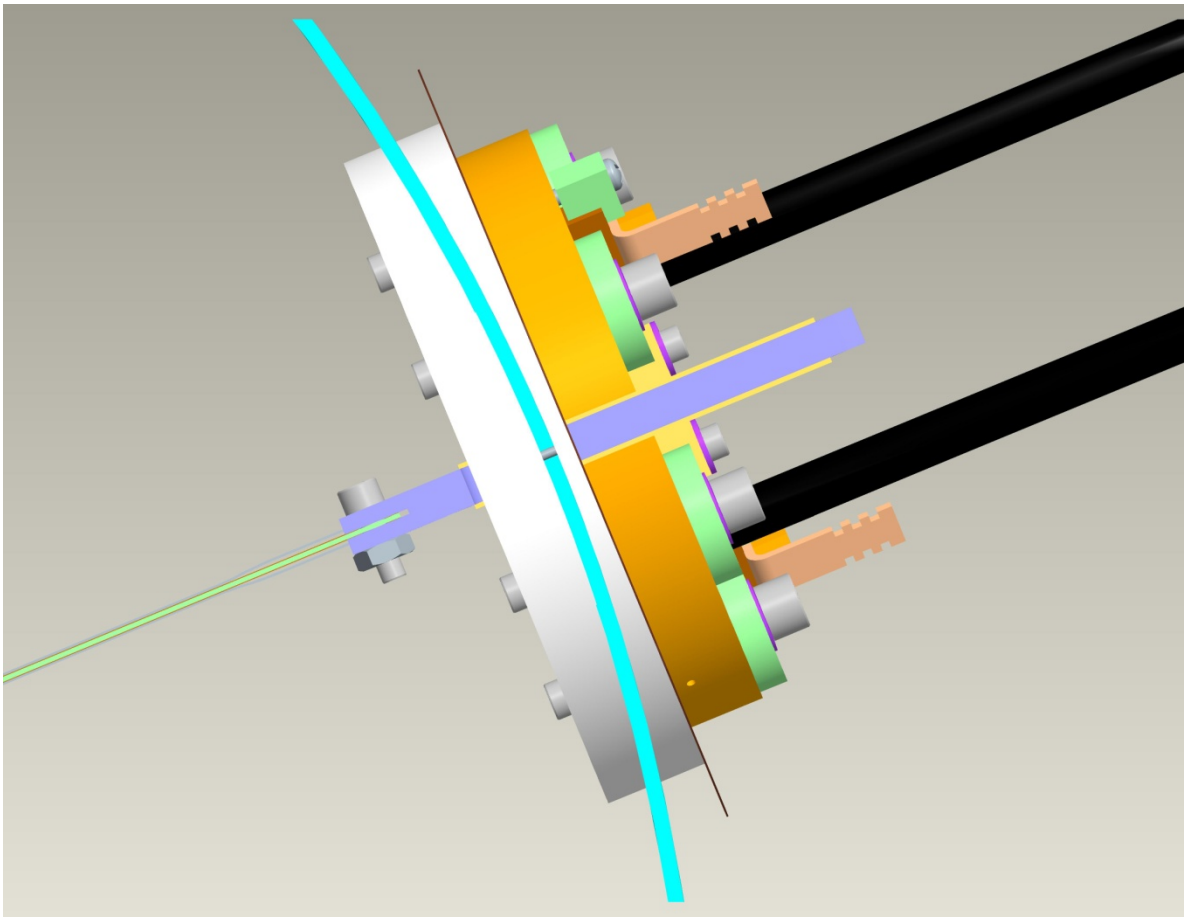

Fig. 2.6 Heat Station – Shield Clamp

The copper terminals provide holes into which the 6 AWG copper wires are soldered, provide tapped holes for mounting temperature sensor and their strain reliefs, provide anchoring for the “warm” end termination parts of the HTS leads, and have through holes that are used to bolt the copper terminals to the aluminum bosses. Fig 2.7 shows a view of the terminals.

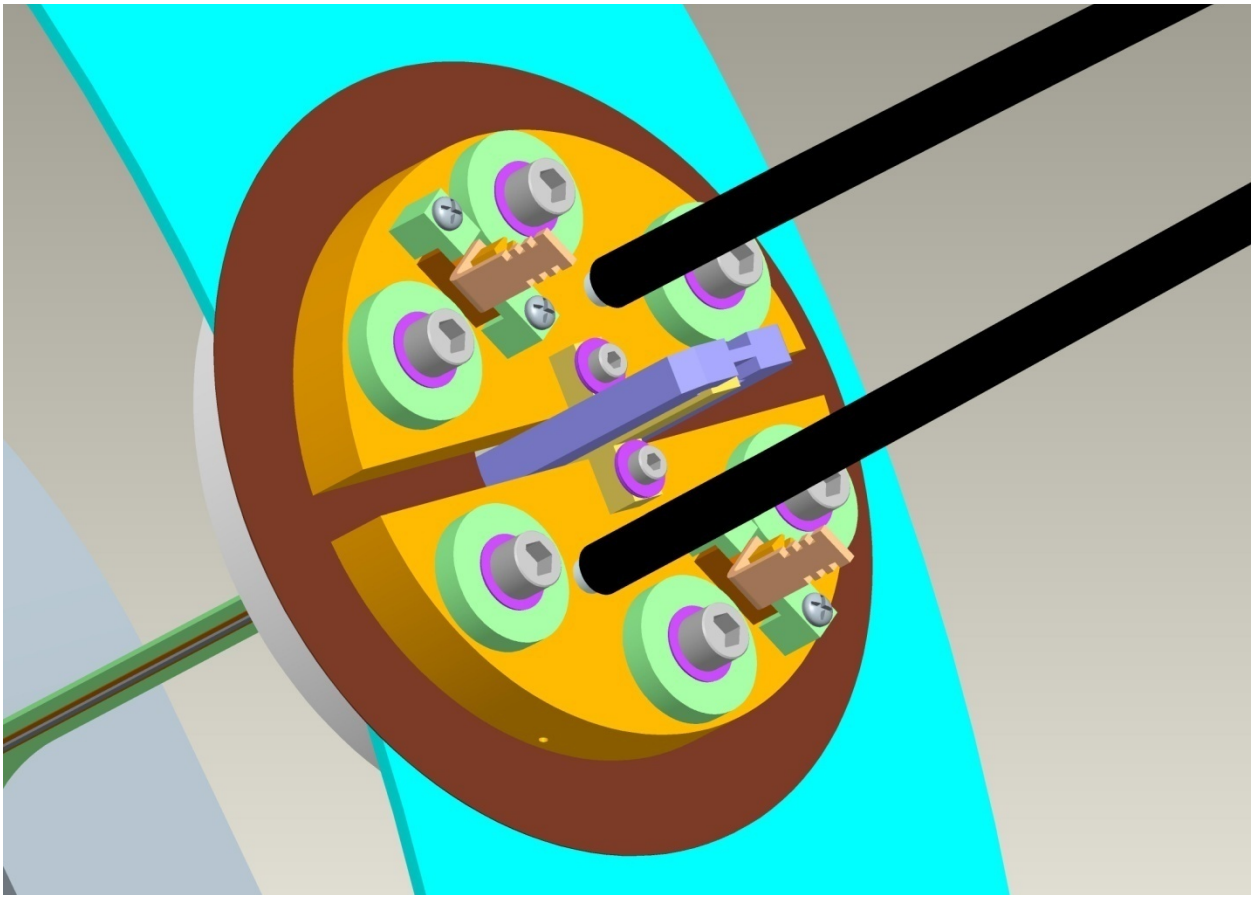

Fig. 2.7 Copper Terminal Pair

The length of the 6 AWG copper wires is determined by designing them as “optimized leads”, meaning the length offers the best compromise between minimized heat conduction ($kA\Delta T/\Delta L \rightarrow$long lead) and minimized internal heat generation ($I^2R \rightarrow$short lead) at the nominal operating current of ~54 A. For 35 A current, the optimum length for 6 AWG wire is 45 inches. The steady state heat load to the shield for each of the four 6 AWG copper wires is expected to be 2.1 W with power on, and 1.0 W with power off (conducted heat only). If the current is kept at ~54 A using the same lead, the increased heat load with power on is expected to be 3.2 W for each lead.

The actual construction of the solenoid assembly has been partially completed. The coils have been wound and tested, and after testing were assembled into their respective yokes. The yoked assembly is scheduled for testing in early 2010. *Fig. 2.**8*** and *Fig. 2.**9*** show two photographs of the partially completed solenoid assembly.

View 1

Fig. 2.8 Completed Solenoid Assembly ready for second cold test

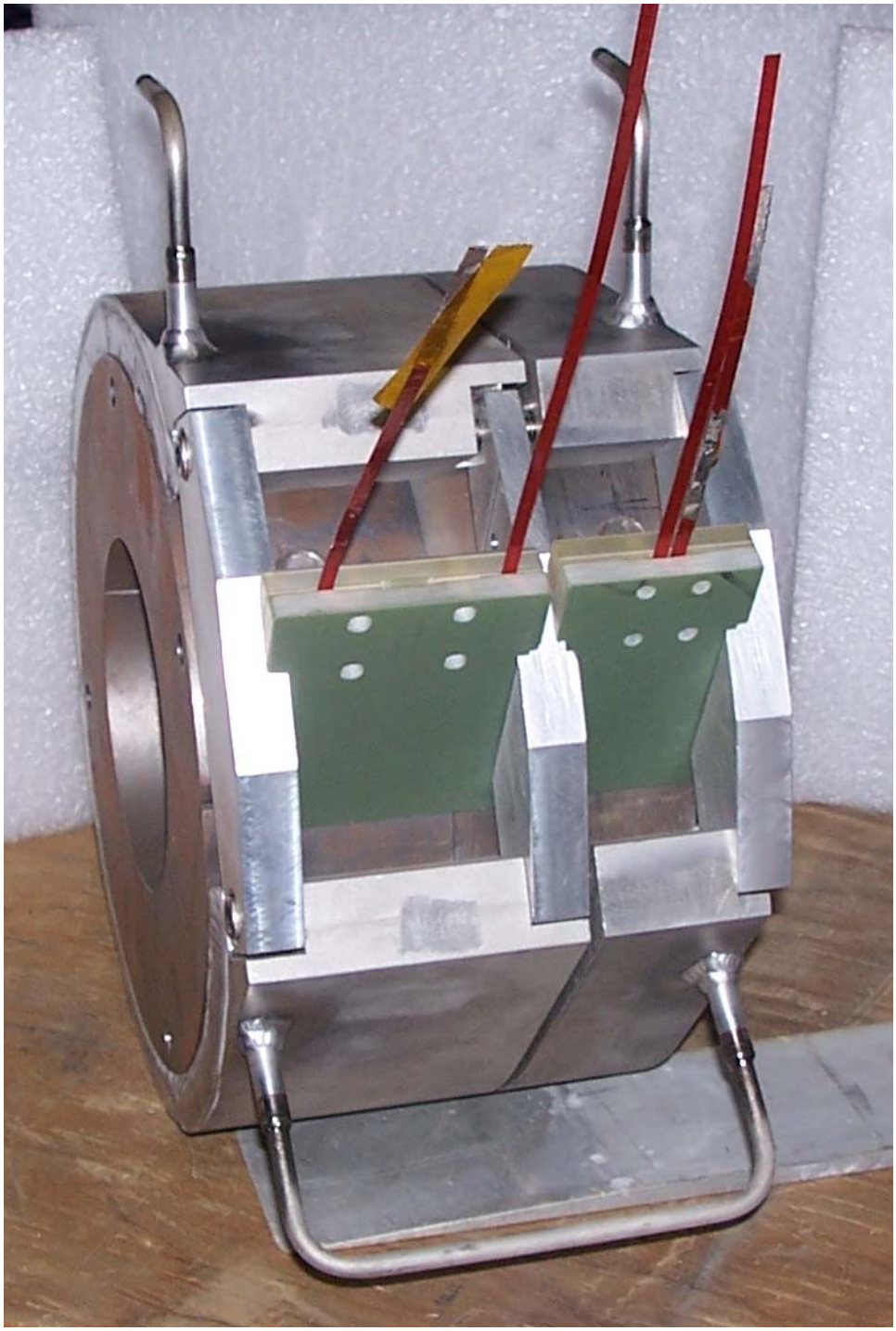

View 2

Fig. 2.9 Completed Solenoid Assembly ready for second cold test

3. Superconducting RF Solenoid and Shielding Experimental Program

An extensive program of magnetic field measurements will be performed with the solenoid assembly at 77 K and a mu-metal shield that simulates the shield to be used during operations to minimize the solenoid fringe field at the RF cavity. The main purpose of these measurements is to verify that the shielding is effective in keeping the fringe field at or below 10 mG when the solenoid is at the maximum operating current of 54.2 A and axial field of ~0.13 T. Measurements of the axial field will also be performed. The fringe field will be measured with a pair of fluxgate probes, and the axial field in the bore of the solenoid with a Hall Effect probe. At the time of this writing, all experimental parts and apparatus had been designed, but the test cryostat, shield, and probe holders were still being machined and assembled. The following text descriptions are therefore accurate, but the photographs of hardware in the figures show the work in progress, not the finished system; however, the images should provide an adequate depiction of the experimental set up.

The solenoid assembly will be immersed in a bath of liquid nitrogen at 77K in a double-walled test cryostat with an outer shell of stainless steel and an inner shell of aluminum, and foam insulation in the space between. The cryostat will not be airtight but fitted with a foam plastic cover of thickness 5.08 cm (2 in) and topped with a Micarta plate of thickness 2.22 cm (7/8 in) with feedthroughs for liquid nitrogen fill and vent lines, level probe, power leads, and voltage taps. The plate will act as a base for a software-controlled vertical transporter that moves the magnetic field probes axially and also rotates them azimuthally (Figs. 3.1 and 3.2). A G-10 warm bore tube with an insulating vacuum jacket will penetrate the cover and plate in order to perform axial field measurements in the solenoid. The photo in Figure 3.3 shows the cryostat with the Micarta plate and warm bore tube in place. The plate and vertical transporter provides enough weight to make a reasonably tight fit for the cover and to minimize the heat load.

Figure 3.1. Vertical transporter and computer control cart.

Figure 3.2. Close up vertical transporter drive mechanisms.

Fig. 3.3. Test cryostat with cover and warm bore tube.

A cylindrical mu-metal shield of height 56.7 cm and inner diameter 61 cm will be installed on top of the Micarta plate in order to simulate the shielding to be used around the RF cavity. The fringe field measurements will be taken within the volume of the cylinder. The shield will also have an opening on its bottom plate through which the warm bore tube will be accessible for axial measurements. Fig 3.4 shows the cryostat assembly with the unfinished shield mounted on top.

Fig. 3.4. Test cryostat with shield in place.

Fringe field measurements will be performed with two Barrington Instruments Mag-01 fluxgate magnetometers with fluxgate low field probes (0-0.2 mT), one of which is axial (Model Mag B) and the other transverse (Model Mag C). Both probes have a field resolution of 1 nT over the range 0-20 μT and 10 nT over the range 20-200 μT. The magnetometer unit has an analog output of ± 5 V (100 μT/V). Fig 3.5 has a photo showing the magnetometer units with their probes and the National Instruments USB 6259 unit which serves as a BNC connection box and 16 bit analog-to-digital-converter (ADC) for data acquisition.

Fig. 3. 5. Fluxgate magnetometers with axial probe (left) and transverse probe (right) and the NI USB ADC /connector unit (far left).

Each fluxgate probe will be mounted in a holder that is designed to slide along a bar that will be mounted on a shaft about which it can rotate and move vertically. This will provide the capability to vary the probe position radially, azimuthally, and axially within the cylindrical shield. Fig 3.6 shows the fluxgate probes in their holders.

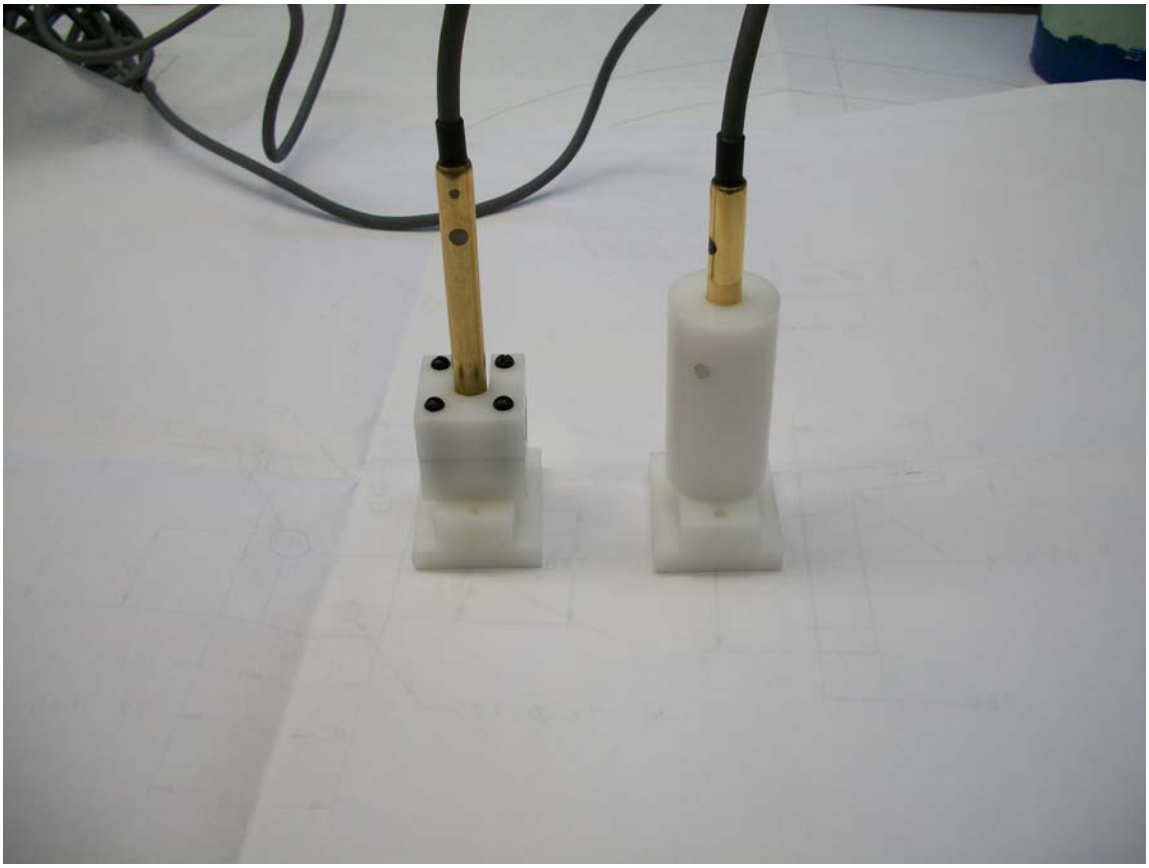

Fig 3.6. Transverse fluxgate probe (left) and axial fluxgate probe (right) in holders.

Axial measurements in the solenoid bore will be performed with a Group3 Technology Model MPT-141-7S Hall Effect probe and Model DTM-151 Teslameter. For the 0 – 0.3 T range of interest, the resolution of the digital output is 0.1 μT. The probe will be mounted on a shaft which can be moved axially along the bore and rotated azimuthally by the vertical transporter, seen in Figs. 3.1 and 3.2.

Data acquisition will be accomplished using LabView software on a local computer which controls two pathways depending on the source of the signals. Analog output from the fluxgate magnetometers, both power supplies (voltage and current), and both solenoids (voltage and current) will be input to the National Instruments USB 6259 ADC and from there written into a data file. Magnetic field data from the Hall probe Teslameter and position and angle data from the vertical transporter is already in digital form and is written directly into the same data file by the LabView program on the local computer. The data included in the data file will be as follows: magnetic field strength and probe position in three dimensions for both fluxgate probes, current and voltage from both power supplies and voltage from both solenoids, Hall probe readings and Hall probe axial position and azimuthal angle from the vertical transporter. The data acquisition system is depicted by the block diagram in Fig 3.7.

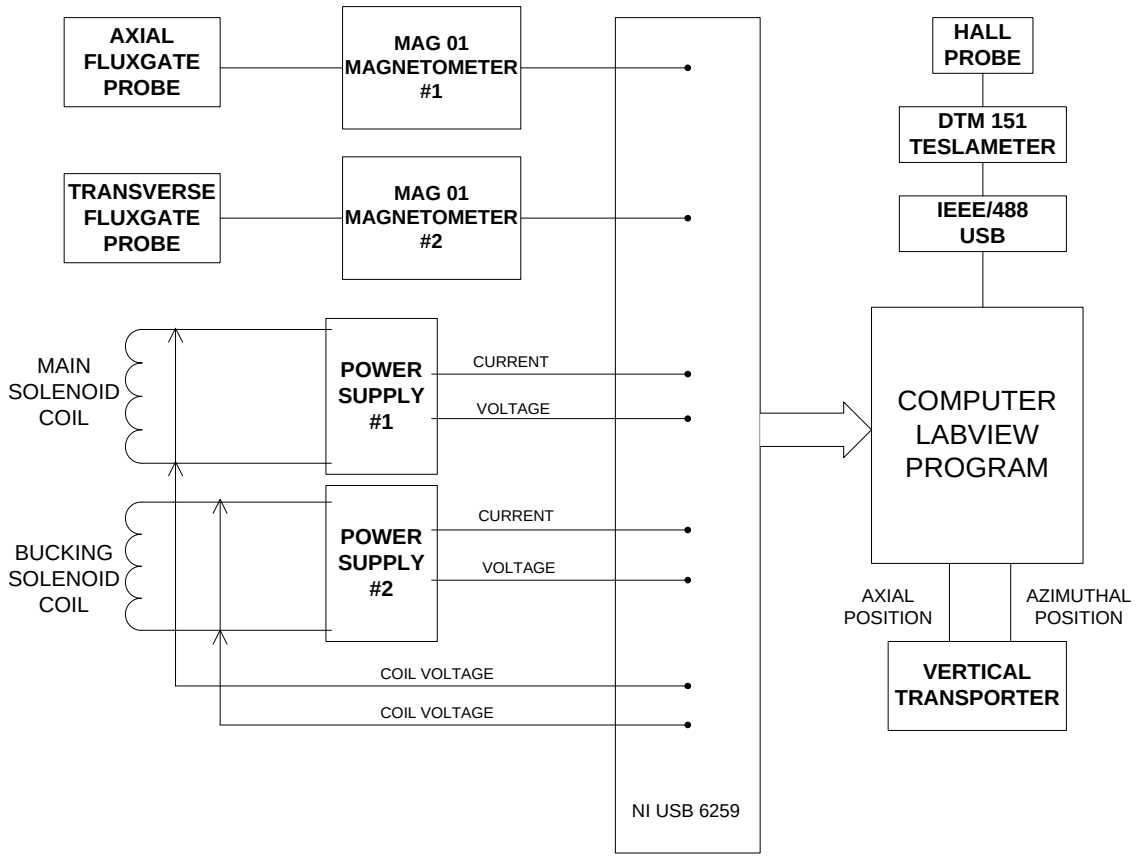

Fig. 3.7. Block Diagram of Measurement and Data Acquisition System

From previous 77 K testing of the solenoid coils to about 65 A without the iron yoke, various parameters to be used for the present experiment have been determined. Quench detection circuits for the two solenoids will generate stop pulses to trigger shutdown of the power supplies when a maximum coil voltage threshold of 1 mV is reached. Maximum test current for the main solenoid and the bucking solenoid is limited to 55 A, as safety margins. In addition, there will be additional safety margin at actual operation where the temperature will be about 5 K.

Selected positions for fringe field measurements depend mainly on the location and configuration of the RF cavity within the cylindrical volume of the shield. These will include the location of furthest radial extent of the RF cavity and the minimum radial extent of the cavity neck, and other positions of interest have been added. The most detailed measurements should be done at the nominal design currents,

54.2 A for the main coil and -17 A for the bucking coil. The selected positions are with respect to the axis and the top of the solenoid, and are designated as follows:

1) radial – center (or nearest possible), 25 mm, 50 mm, 75 mm, 100 mm, 125 mm, 150 mm, 175 mm, 200 mm, 225 mm
2) axial – 160, 190, 220, 250 mm from the top surface of the iron
3) azimuthal – 60 deg steps

For less detailed measurements, the positions are

1) radial – 50 mm, 200 mm
2) axial – 160, 190, 220, 250 mm from the top surface of the iron
3) azimuthal – 120 deg steps

With these selected test parameters in mind, a test plan can be outlined as followed.

1) Electrical checkout at room temperature.

2) Cooldown to 77K.

3) Electrical checkout at 77K.

4) Power supply shutdowns with manual trips to verify quench detection operation.

5) Hall probe axial measurements with solenoids unpowered.

6) Fluxgate measurements of fringe field at selected positions with solenoids unpowered.

7) Ramp main solenoid to 54.2 A at 1 A/s with steps to monitor coil voltage.

8) Ramp bucking solenoid to -17 A at 0.1 A/s with steps to monitor coil voltage.

9) Axial scan with Hall probe at selected positions.

10) Fluxgate measurements of fringe field at selected positions.

11) With the main solenoid at 54.2 A repeat measurements in steps 9-10 with the bucking solenoid at 0 A and similarly with the bucking coil at -17 A, repeat measurements in steps 9-10 with the main solenoid at 0 A.

12) With the main solenoid at 54.2 A, repeat measurements in steps 9-10 with the bucking solenoid at the following other current levels (opposite polarity): - 0, 8.5, 13, 15, 17, 19, 21 A in the bucking coil.

[i] Master Bond, Inc., formulation EP37-3FLFAO-ND

References:

[1] American Superconductor Corporation, http://www.amsc.com/.